Electronic Supplementary Information

CdS Nanocages@Defective-CoNi-LDH with Bilayer Porous Hollow Frameworks toward Optimized Sono-Photocatalytic Performance

Bin Fang[a], Zipeng Xing[a,*], Fan Du[a,c], Weifeng Kong[a], Zhenzi Li[b,*], Wei Zhou[a,b,*]

[a] Department of Environmental Science, School of Chemistry and Materials Science, Heilongjiang University, Harbin, 150080 P. R. China
[b] Shandong Provincial Key Laboratory of Molecular Engineering, School of Chemistry and Chemical Engineering, Qilu University of Technology (Shandong Academy of Sciences), Jinan 250353, P. R. China
[c] Heilongjiang Suihua Ecological Environmental Monitoring Centre, Suihua, P. R. China
*Corresponding author: Email: xingzipeng@hlju.edu.cn; zzli@qlu.edu.cn; zwchem@hotmail.com

Experimental Section

Characterizations

The powder X-ray diffraction (XRD) patterns were acquired on a Bruker D_8 Advance diffractometer by using Cu Kα radiation (λ = 1.5406 Å). Scanning electron microscopy (SEM) images were obtained with a Philips XL-30-ESEM-FEG instrument operating at 20 kV. Transmission electron microscope (TEM) JEOL JEM-2010 at an accelerating voltage of 200 kV was also used to record the electron micrographs of the samples. X-ray photoelectron spectroscopy (XPS) was measured on a PHI-5700 ESCA instrument with Al-Kα X-ray source. UV-vis diffuse reflection spectra (DRS) were recorded on a UV-vis spectrophotometer (UV- 2550, Shimadzu) with an integrating sphere attachment, and $BaSO_4$ was used as the reference material. Brunauer-Emmett-Teller (BET) surface areas were determined using N_2 adsorption-desorption isotherms measured on a Quanta chrome Autosorb-1C analyzer. The •OH radicals were detected by the fluorescence probe technique with terephthalic acid (TA) on a RF-5301PC fluorescence spectrophotometer. The steady-state photoluminescence (PL) spectra were measured with a PE LS 55 spectrofluorophotometer at excitation wavelength of 350 nm. Fourier transform infrared (FT-IR) spectra were recorded on a Perkin Elmer FT-IR spectrophotometer to get the fingerprint of the chemical bonding vibration of the material. The work function of samples was tested by Scanning Kelvin probe (SKP) (SKP5050 system, Scotland). The electron spin resonance (ESR) spectra under visible light irradiation were tested with ESR spectrometer (Bruker model A300). The measurements were conducted in dichloromethane solution containing 0.1 M TBAPF6. Current-voltage (I-V) curves and photocurrent response were measured by a CHI760E potentiostat. The electrochemical impedance spectroscopy (EIS) measurements and Mott-Schottky plots were performed on an electrochemical workstation in the presence of Na_2SO_4 (100 mM, pH= 6.8).

Photocatalytic activity evaluation

H_2 evolution

The photocatalytic H_2 evolution experiments were performed in a 300 mL Pyrex glass reactor based on an online system (Labsolar-6A, Perfect Light, Beijing). In a typical experimental procedure, 10 mg of photocatalysts was dispersed into the mixed aqueous solution with 10 mL TEOA (hole sacrificial agent) and 90 mL water (5wt. % Pt was in-situ photo-deposited on the surface of samples as co-catalyst), and one ultrasonic vibrating rods (20 W, 10 kHz) were placed right next to the beaker wall. Next, the above mixture solution was degassed thoroughly to remove air and irradiated by a 300 W Xenon commercial lamp. Finally, the generated H_2 was sampled and quantified with an online gas chromatograph (GC D7900P, TCD detector).

Bisphenol A (BPA) degradation

The photocatalytic degradation of BPA experiments was conducted in a 100 mL reactor including 50 mL 20 ppm BPA aqueous solution and 20 mg of the prepared photocatalyst. After vigorously stirring for 30 min in the dark to reach adsorption-desorption equilibrium, the suspensions were irradiated by a 300 W Xenon

commercial lamp, and one ultrasonic vibrating rod (20 W, 10 kHz) were placed right next to the beaker wall. At designated time intervals, 1.5 mL of suspension was sampled and filtered with a 0.22 μm membrane to remove the residual particles. Finally, the BPA content was measured colorimetrically at 276 nm using diphenyl carbazide (DPC) method on a Shimadzu UV-vis 3600 spectrophotometer.

Apparent quantum efficiency (AQE)

AQE for H_2 production was measured using monochromatic light and calculated using the following formula:

$$AQE = \frac{N_e}{N_p} \times 100\% = \frac{2 \times N \times N_A}{\frac{E_{total}}{E_{photon}}} \times 100\%$$

$$= \frac{2 \times N \times N_A}{\frac{S \times P \times t}{h \times \frac{C}{\lambda}}} \times 100\% = \frac{2 \times N \times N_A \times h \times c}{S \times P \times t \times \lambda} \times 100\% \quad (S1)$$

Where, N represents the amount of produced H_2 molecules (mol), N_A is the Avogadro constant (6.022×10^{23}), h represents the Planck constant (6.626×10^{-34} J·s), c is the speed of light (3×10^{8} m/s), S is the irradiation area (cm^2), P is the intensity of irradiation light ($mW\cdot cm^{-2}$), t is the photoreaction time(s), λ is the wavelength of the incident monochromatic light (m).

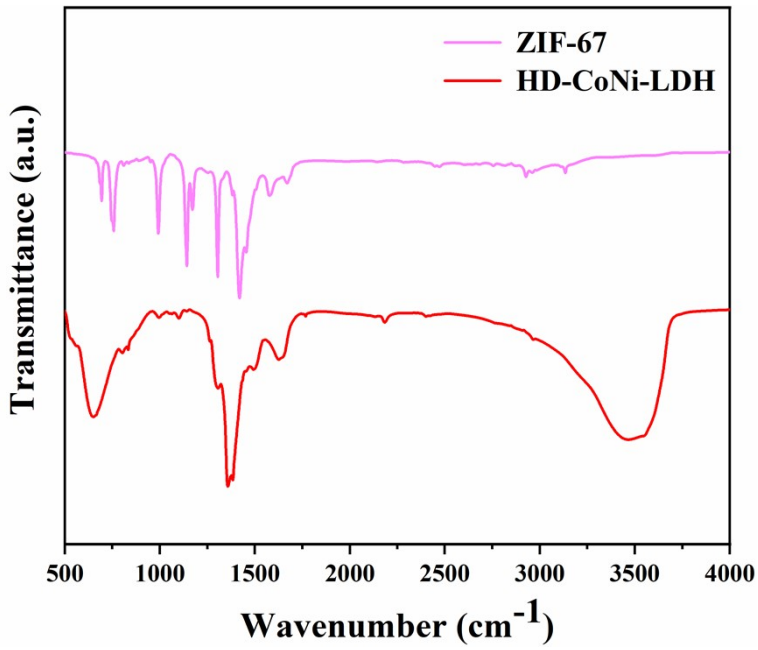

Figure S1. FT-IR spectra of ZIF-67 and HD-NiCo-LDH.

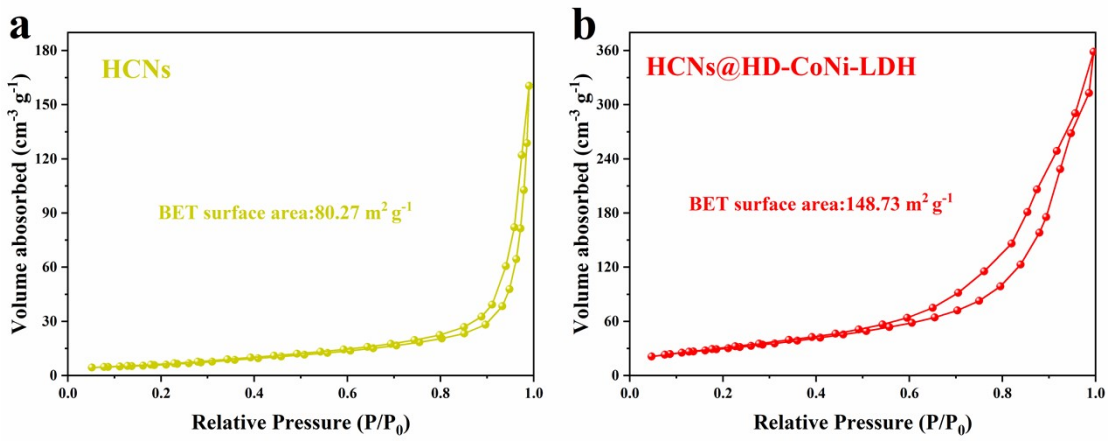

Figure S2. N_2 adsorption-desorption isotherms for as-prepared (a) HCNs and (b) HCNs@HD-CoNi-LDH.

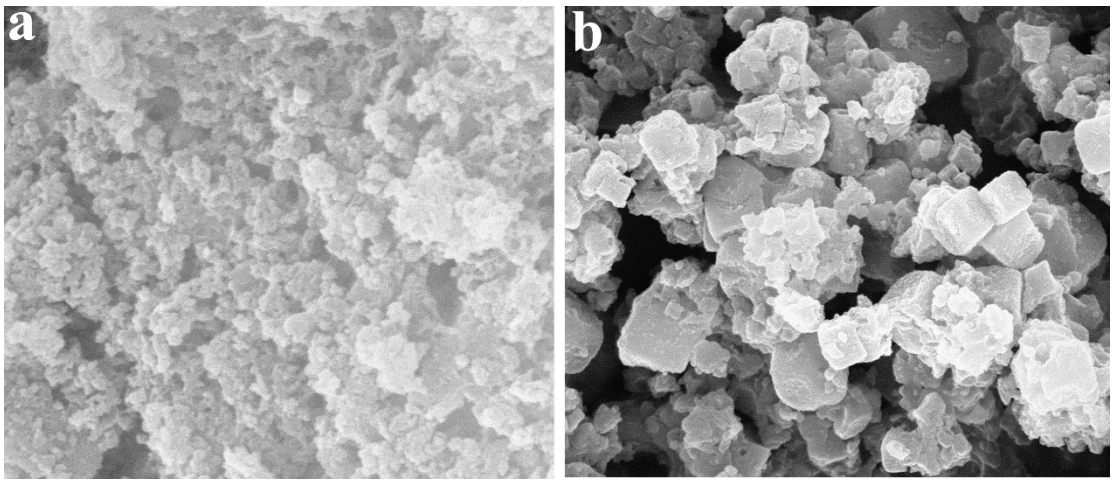

Figure S3. SEM images of Bulk-CoNi-LDH (a) and HCNs-Bulk-CoNi-LDH (b).

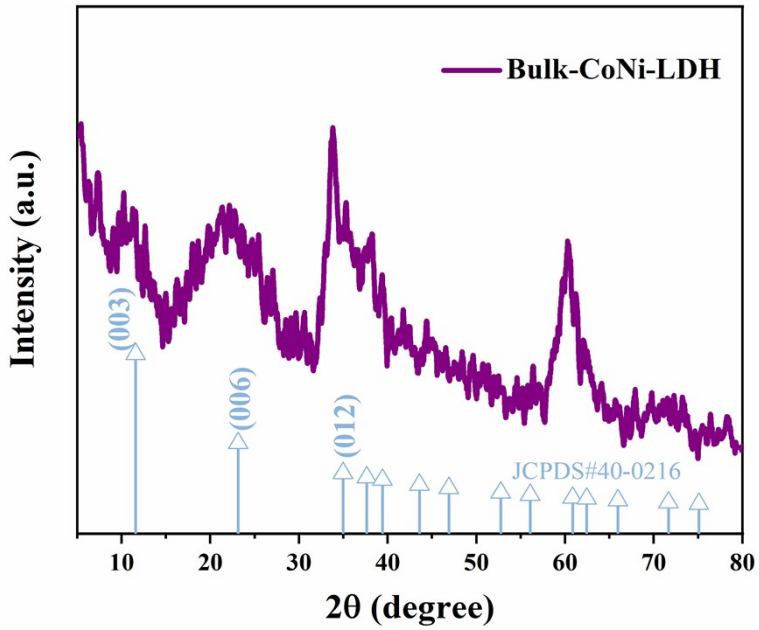

Figure S4. XRD pattern of Bulk-CoNi-LDH.

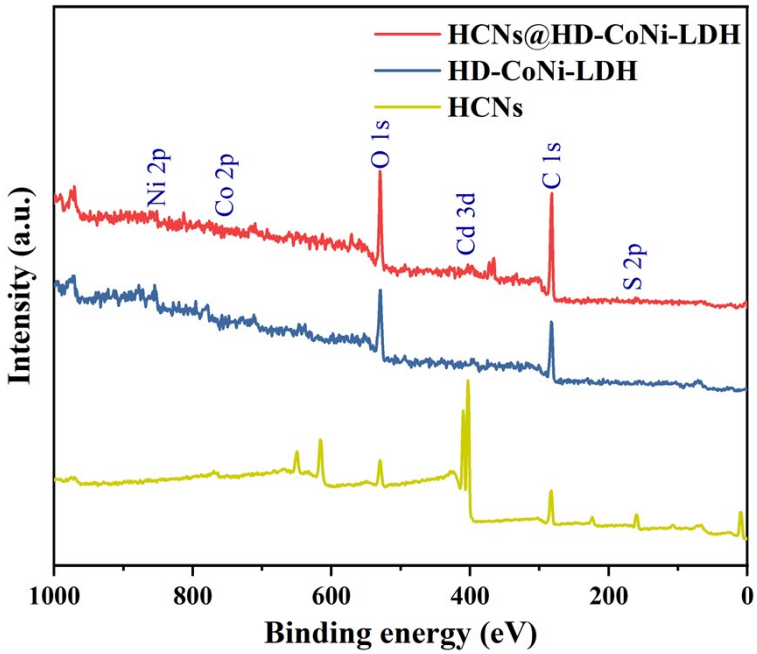

Figure S5. XPS spectra of HCNs@HD-CoNi-LDH, HD-CoNi-LDH and HCNs: full survey.

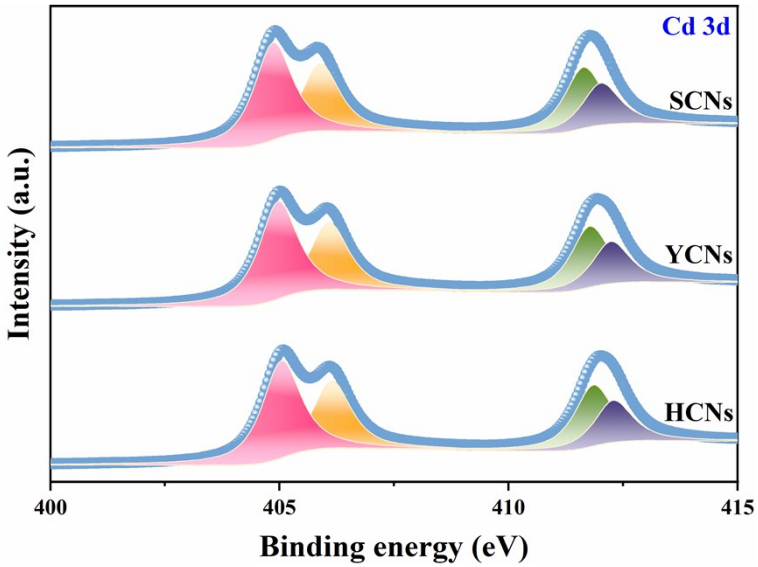

Figure S6. XPS spectra of Cd 3d for SCNs, YCNs and HCNs, respectively.

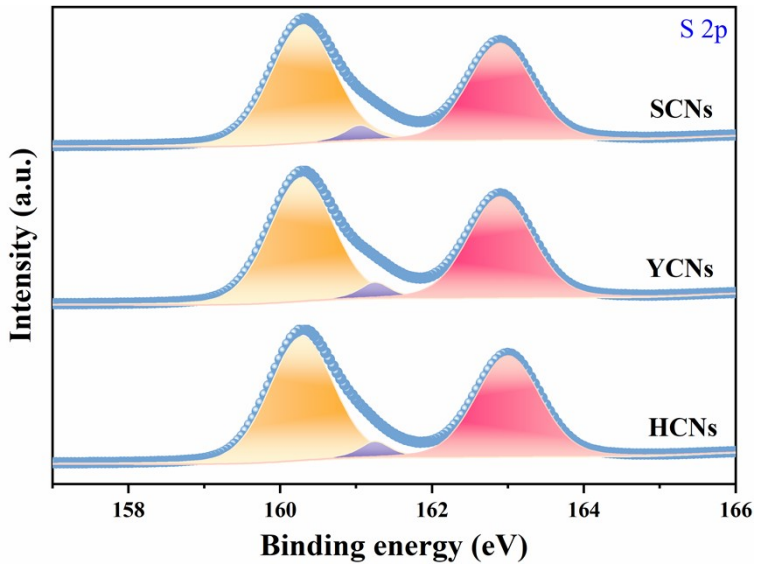

Figure S7. XPS spectra of S 2p for SCNs, YCNs and HCNs, respectively.

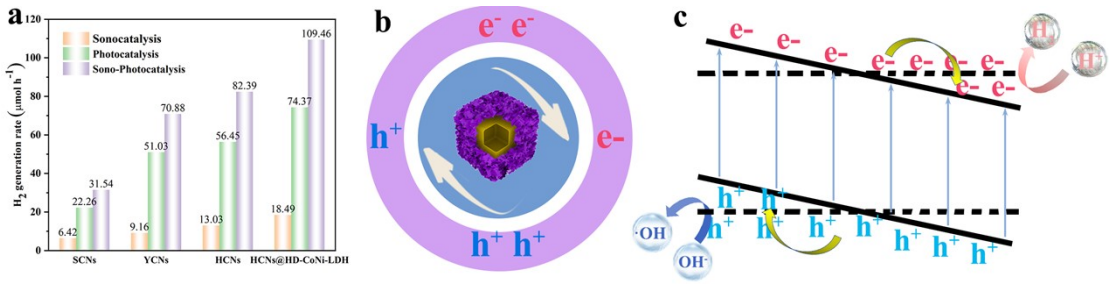

Figure S8. (a) The sonocatalytic, photocatalytic and sono-photocatalytic hydrogen production rate of the prepared samples. (b-c) Schematic for the sono-photocatalytic process of HCNs@HD-CoNi-LDH and the energy band diagram of HCNs@HD-CoNi-LDH heterostructure under both UV irradiation and ultrasonic.

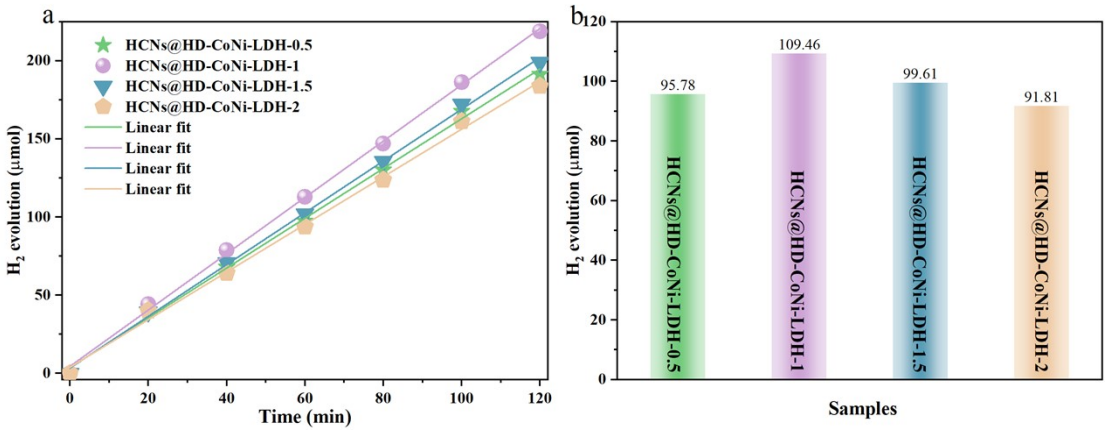

Figure S9. (a) The sono-photocatalytic hydrogen evolution of HCNs@HD-CoNi-LDH-x (x=0.5, 1, 1.5 and 2) with time under visible light irradiation. (b) Sono-Photocatalytic hydrogen production rates of the prepared HCNs@HD-CoNi-LDH-x composites.

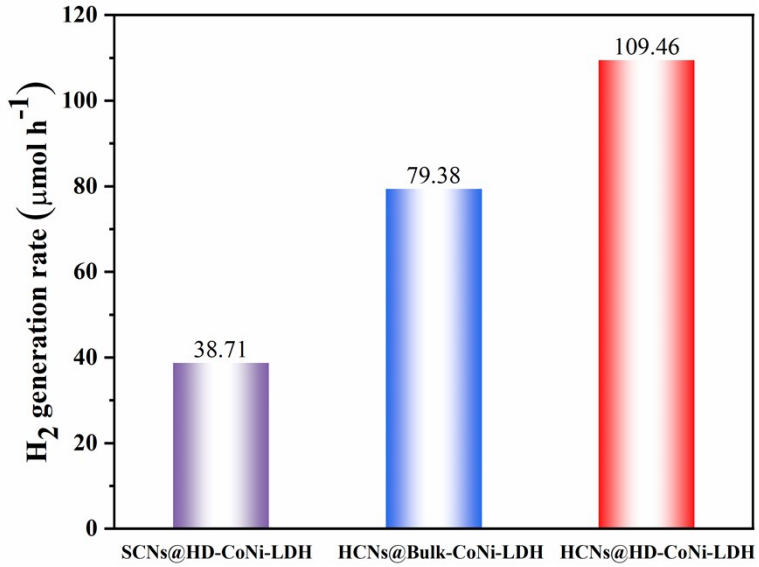

Figure S10. Sono-Photocatalytic hydrogen production rates of the prepared SCNs@HD-CoNi-LDH, HCNs@Bulk-CoNi-LDH and HCNs@HD-CoNi-LDH composites under visible light irradiation.

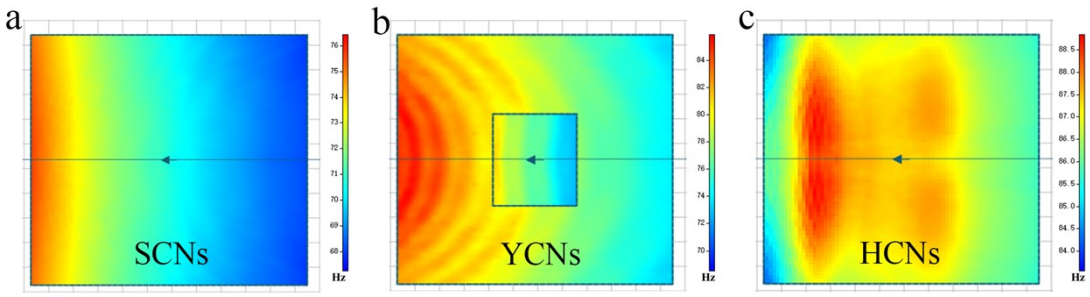

Figure S11. Schematic diagram of simulated sound field of SCNs, YCNs and HCNs.

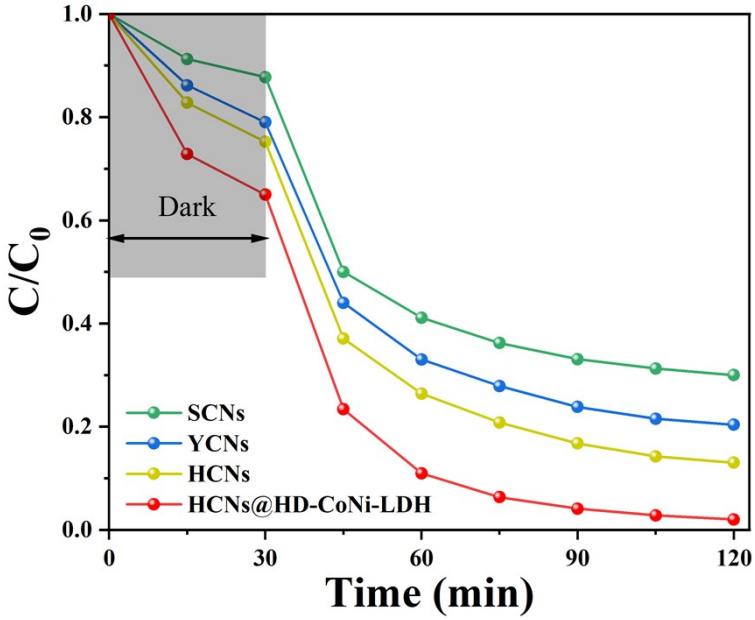

Figure S12. Sono-Photocatalytic degradation of BPA in aqueous solution for different samples under visible light irradiation.

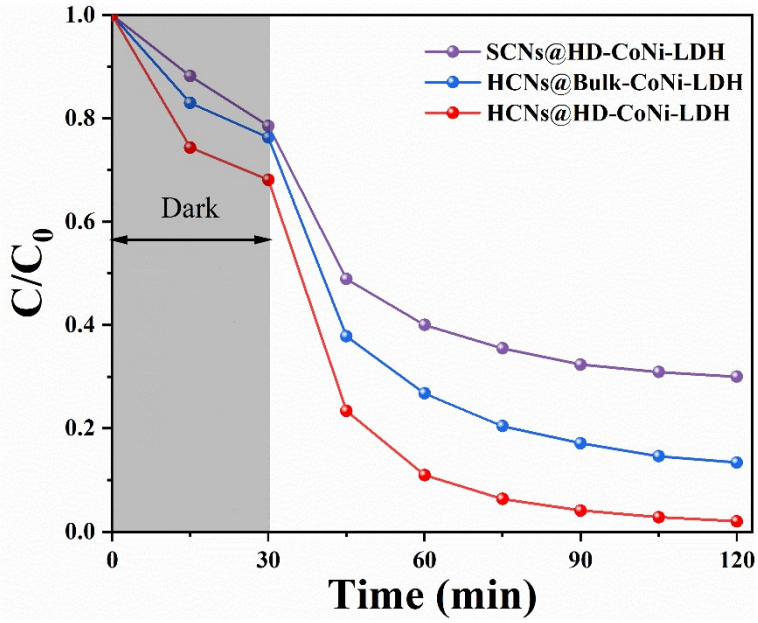

Figure S13. Sono-Photocatalytic degradation of BPA in aqueous solution for different samples under visible light irradiation.

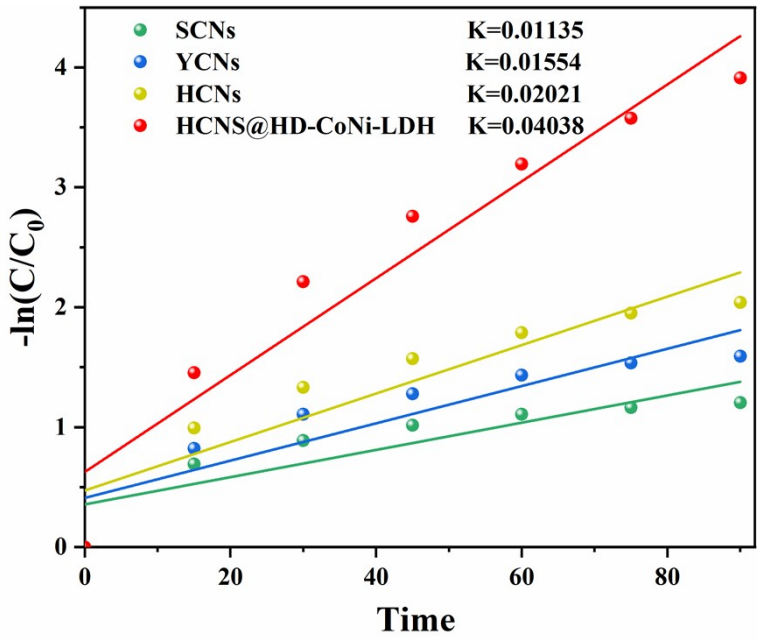

Figure S14. Sono-Photocatalytic degradation plots with the apparent reaction rate constants K for the degradation of BPA.

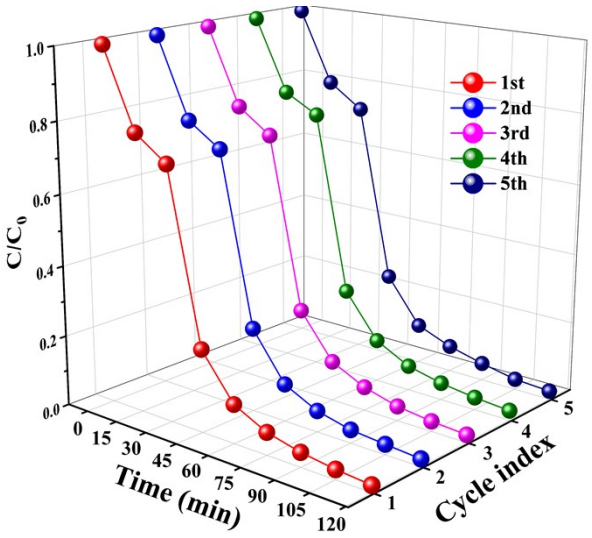

Figure S15. Cycling tests of sono-photocatalytic degradation of BPA by HCNs@HD-CoNi-LDH composites.

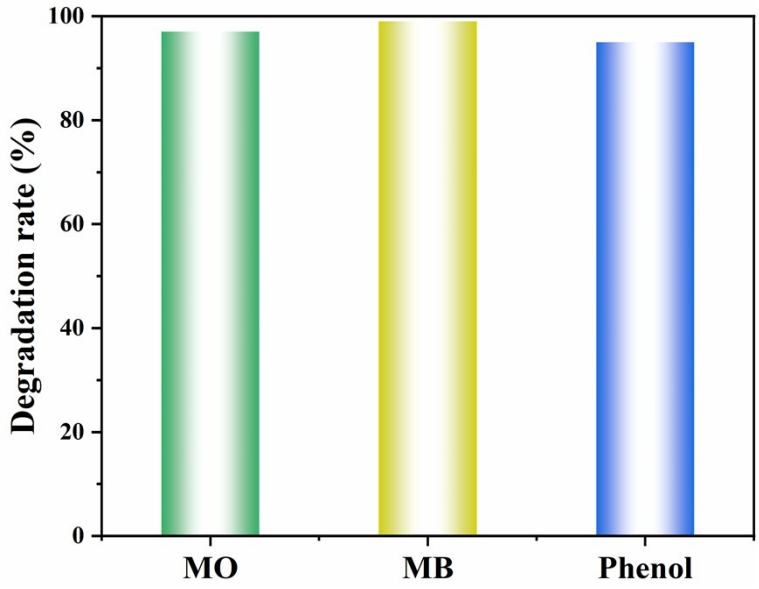

Figure S16. Sono-Photocatalytic degradation rates of HCNs@HD-CoNi-LDH for different pollutants within 120 min degradation process.

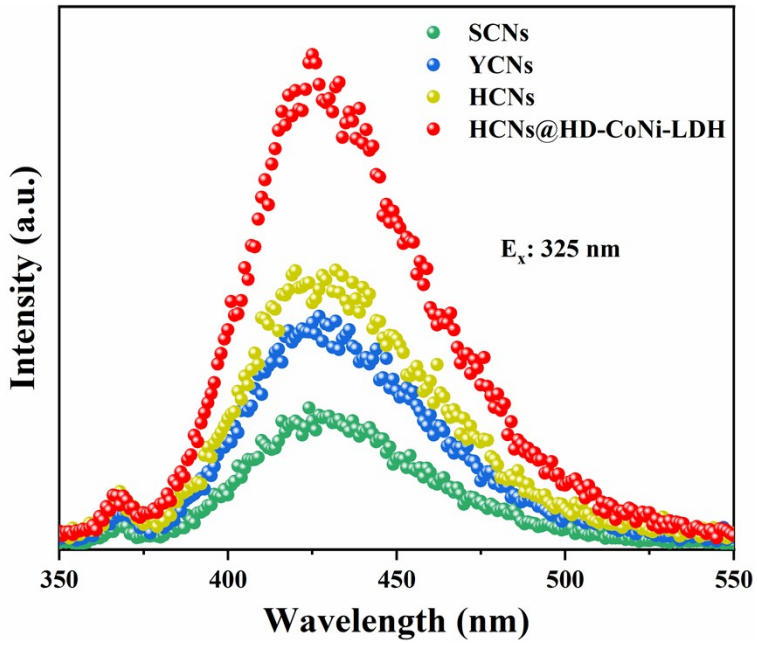

Figure S17. Fluorescence spectra related to the amount of produced •OH for SCNs, YCNs, HCNs and HCNs@HD-CoNi-LDH.

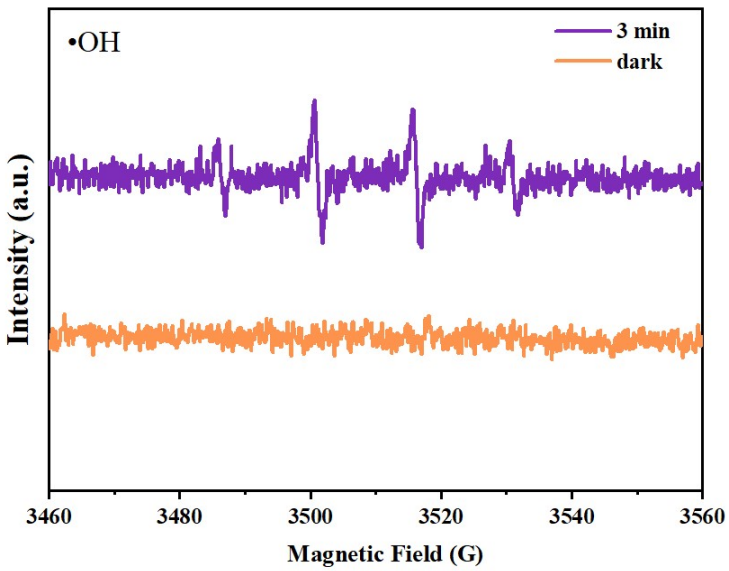

Figure S18. ESR spectra of DMPO-•OH in the dark and visible light irradiation for 3 min.

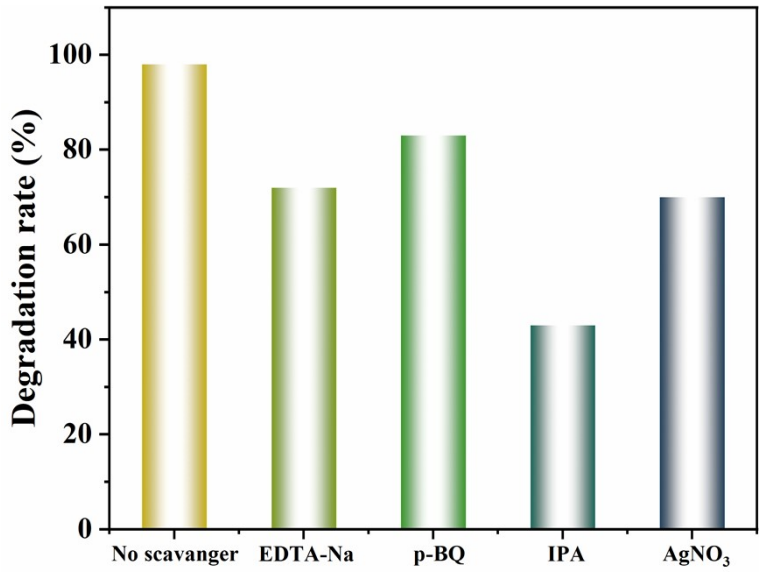

Figure S19. The species trapping experiments for sono-photocatalytic degradation of BPA over HCNs@HD-CoNi-LDH photocatalyst under visible light irradiation.

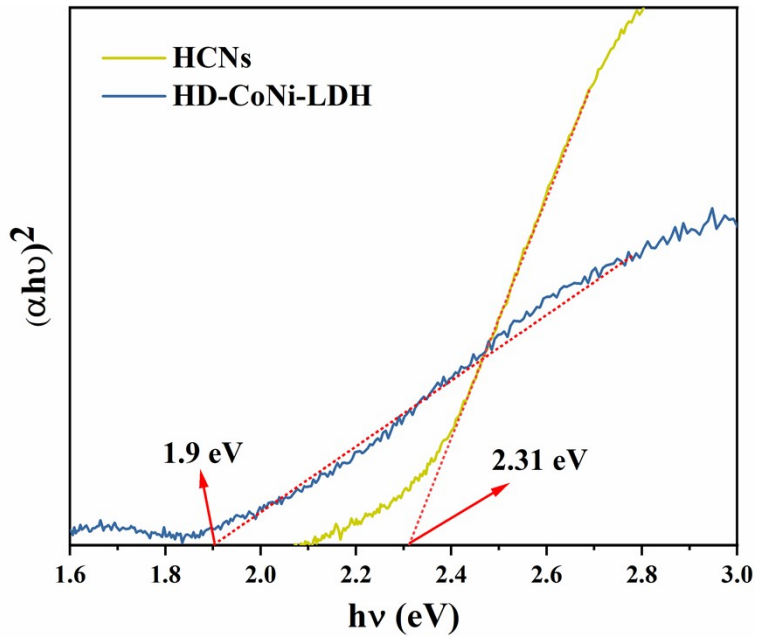

Figure S20. Plots of $(\alpha h\nu)^2$ vs. $h\nu$ for HCNs and HD-CoNi-LDH samples.

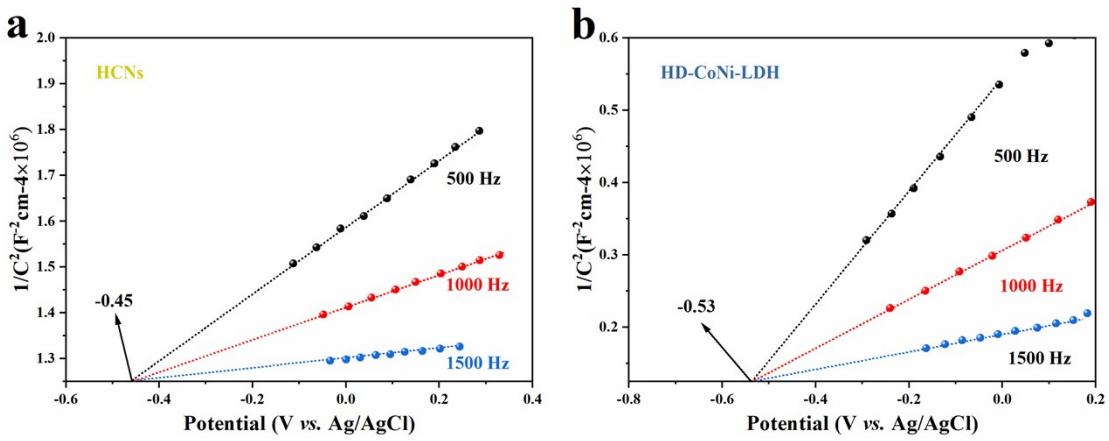

Figure S21. Mott-Schottky plots of HCNs (a) and HD-CoNi-LDH samples (b) under different frequency.

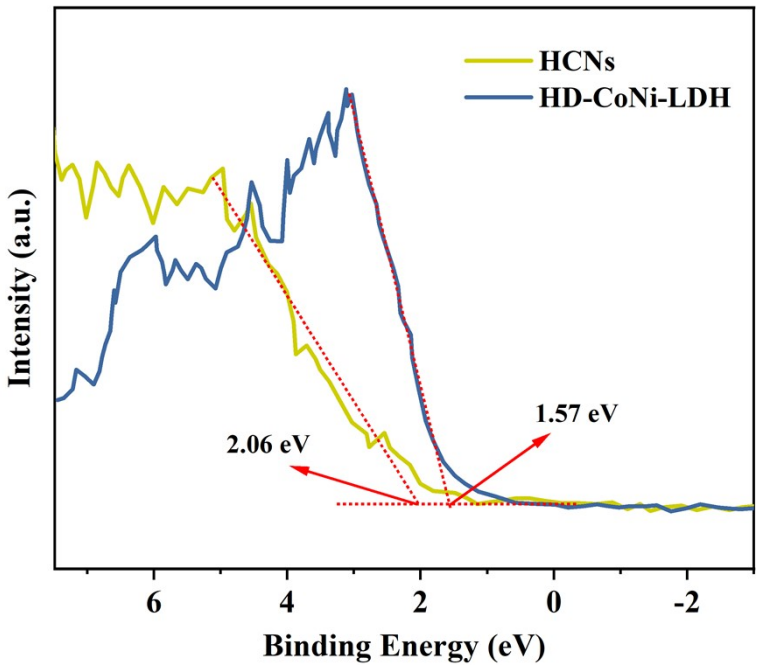

Figure S22. VB XPS spectra of HCNs and HD-CoNi-LDH, respectively.

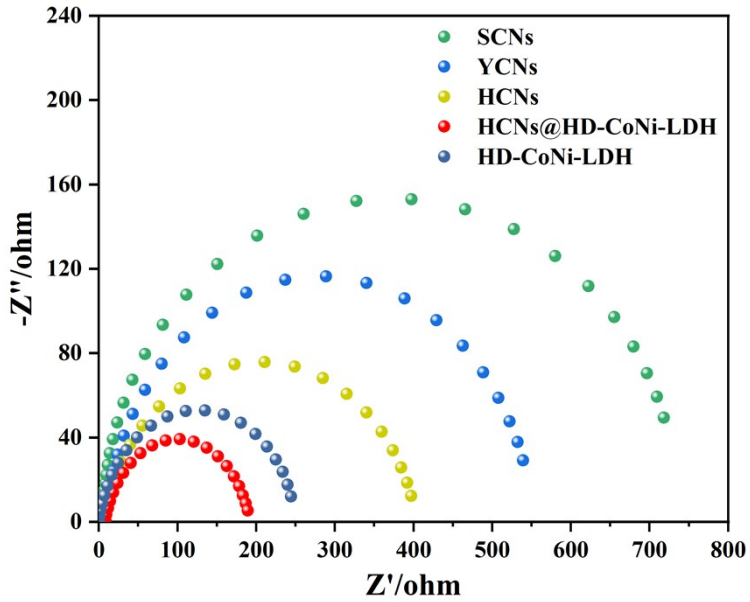

Figure S23. EIS data for different samples.

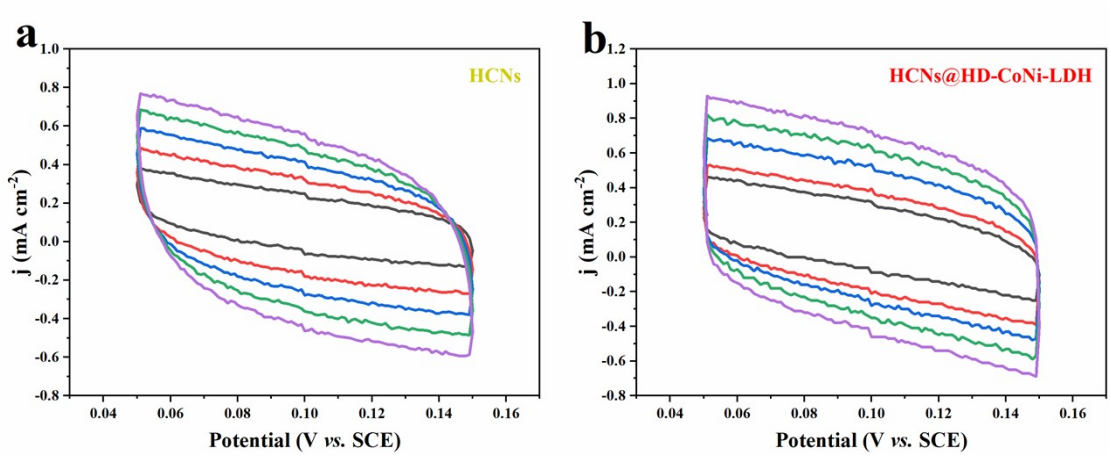

Figure S24. Cyclic voltammogram tests of HCNs and HCNs@HD-NiCo-LDH using different scan rates (10, 20, 30, 40, 50 $mV \cdot s^{-1}$, respectively).

Table S1. The AQE values of the HCNs@HD-CoNi-LDH photocatalysts at different single-wavelengths.

Wavelength (nm)	H_2 evolution (μmol)	Light intensity P ($mW \cdot cm^{-2}$)	AQE (%)
420	1082.48	26.42	7.32
450	952.65	26.93	5.90
500	418.08	27.2	2.31
600	185.17	28.14	0.82
700	62.76	26.86	0.25

Table S2. The band gap energies, conduction band (CB) and valence band (VB) potentials (NHE) for HCNs and HD-CoNi-LDH.

Sample	Band gap (eV)	CB (eV)	VB (eV)
HCNs	2.31	-0.25	2.06
HD-CoNi-LDH	1.9	-0.33	1.57

Table S3. Comparison of H_2 generation rates of HCNs@HD-CoNi-LDH photocatalysts and literatures.

Catalysts	Light Source	H_2 (mmol·h^{-1} g^{-1})	AQE	Ref.
CdS@CoNi-LDH	**Xe Lamp (300W, λ≥420 nm)**	**10.946**	**7.32%（420nm）**	**This work**
g-C_3N_4/CdS	Xe Lamp (300W, λ≥420 nm)	1.809	2.79% (420 nm)	1
CdS	Xe Lamp (300W, λ≥420 nm)	0.434	0.43% (420 nm)	2
CdS/NiOOH	Xe Lamp (300W, λ≥420 nm)	0.1186	3.67% (420 nm)	3
CdS/BCNNTs	Xe Lamp (300W, λ≥420 nm)	0.526	4.01% (420 nm)	4
CdS-Pd	Xe Lamp (300W, λ≥420 nm)	0.9479	4.47% (420 nm)	5
CdS-fullerene/graphene	Xe Lamp (300W, λ≥420 nm)	0.1272	7.24% (420 nm)	6
WO_3/CdS/WS_2	Xe Lamp (300W, λ≥420 nm)	9.55	5.49% (475 nm)	7
CdS@$ZnIn_2S_4$	Xe Lamp (300W, λ≥400 nm)	0.6048	1.63% (400 nm)	8

References:

1. Z. Wang, Z. Wang, X. Zhu, C. Ai, Y. Zeng, W. Shi, X. Zhang, H. Zhang, H. Si, J. Li, C.-Z. Wang and S. Lin, *Small*, 2021, **17**, 2102699.
2. Y. Wang, J. Zhao, W. Hou and Y. Xu, *Appl. Catal. B-Environ.*, 2022, **310**, 121350.
3. W. Chen, G.-B. Huang, H. Song and J. Zhang, *J. Mater. Chem. A*, 2020, **8**, 20963-20969.
4. Z. Ai, K. Zhang, D. Shi, B. Chang, Y. Shao, L. Zhang, Y. Wu and X. Hao, *Nano Energy*, 2020, **69**, 104408.
5. W. Li, X.-s. Chu, F. Wang, Y.-y. Dang, X.-y. Liu, T.-h. Ma, J.-y. Li and C.-y. Wang, *Appl. Catal. B-Environ.*, 2022, **304**, 121000.
6. W. Wang, Y. Tao, J. Fan, Z. Yan, H. Shang, D. L. Phillips, M. Chen and G. Li, *Adv. Funct. Mater.*, 2022, **32**, 2201357.
7. C. Xue, P. Zhang, G. Shao and G. Yang, *Chem. Eng. J.*, 2020, **398**, 125602.
8. E. Zhang, Q. Zhu, J. Huang, J. Liu, G. Tan, C. Sun, T. Li, S. Liu, Y. Li, H. Wang, X. Wan, Z. Wen, F. Fan, J. Zhang and K. Ariga, *Appl. Catal. B-Environ.*, 2021, **293**, 120213.